Patterns of load distribution among the legs in small water striders during standing and striding

J. Meshkani[1] (ID), H. Rajabi[2], A. Kovalev[1] & S. N. Gorb[1]

[1]Department of Functional Morphology and Biomechanics, Institute of Zoology, Kiel University, Kiel, Germany
[2]Division of Mechanical Engineering and Design, School of Engineering, London South Bank University, London, UK

Abstract

Water striders (*Gerris argentatus*) move across the water surface by taking advantage of the surface tension, which supports their bodyweight without breaking. During locomotion, the midlegs are primarily responsible for generating thrust, whereas the other legs support the body. Although the aspects of standing and locomotion on the water surface are well understood, relatively fewer studies concerned the coordinated biomechanical movements of the legs. In order to maintain buoyancy of the body on the water surface, the leg positions must be adjusted to distribute the bodyweight appropriately. The present study investigates distribution of the bodyweight on the legs in relatively small water striders. We aimed to understand how loading on the legs changes during sculling that leads to sliding of the body on the water surface. The assistance of all legs at every moment enables the body to maintain its floating during standing and striding. Water striders can achieve a gentle striding through the midlegs driving phase in association with smooth load shifting among their legs, which are positioned in a specific configuration to support the insect on the water surface.

Introduction

Water striders (*Gerris argentatus*) inhabit a wide variety of environments, including the surface of calm and turbulent waters (Andersen, 1982). The cohesive property of water molecules allows the water surface to resist the weight of water striders (Denny, 2004; Vinnichenko et al., 2018). Their bodyweight is supported by the legs, which possess a high level of hydrophobicity (Bush et al., 2007; Caponigro & Eriksen, 1976; Feng et al., 2007; Gao & Jiang, 2004; Hu & Bush, 2010). Water striders perform locomotion to escape or explore their environment in search of nutrients and mates (Krupa & Sih, 1993; Ortega-Jimenez et al., 2017; Waldbauer, 2006). Their movements on water are adapted to several locomotion modes. In addition to jumping, in which the body moves nearly vertically, water striders stride slowly by sculling while their legs remain in contact with water and traverse rapidly by leaping above the surface (Andersen, 1976; Baek et al., 2020; Caponigro & Eriksen, 1976; Hu & Bush, 2010; Kim et al., 2017; Koh et al., 2015; Ortega-Jimenez et al., 2017). Striding, as the type of locomotion that we have focused on it in this study, involves extensive changes in the body posture and load spreading on the legs (Bush & Hu, 2006; Lu et al., 2018). With their locomotion adaptation, they can reach a high velocity with minimum energy expenditure (Rinoshika, 2012). Water striders can, therefore, be used as a model to study the biomechanical aspects of sculling in insects.

Water striders exhibit a variety of body postures that can be classified as static and dynamic states.

Previous studies showed that water striders can adjust their legs effectively in order to stand on the water surface and carry out locomotion activities efficiently (Baek et al., 2020; Yang et al., 2016). A comprehensive understanding of the role that the legs play in supporting the body in various postures, particularly in the dynamic state, requires assessing the load distribution pattern and considering leg alignment changes.

At the standstill position, each leg pushes water down so that the surface is indented, and a dimple appears. The topography of the deformed water can be assessed accurately by using the Schlieren method, which demonstrates a linear relationship between loading magnitude and the dimensions of the dimple (Moisy et al., 2009; Steinmann et al., 2018). In this context, the weight of the displaced fluid is equal to the load exerted on the air–water interface, which can be used as a basis for estimating the mass of water-walking insects (Hu & Bush, 2010; Keller, 1998; Steinmann et al., 2018).

The distorted water surface can be detected by a black spot with a bright perimeter on the bottom of the bodywater that is

created due to the refraction of light passing through the fluid (Kiehn, 2007). Shadows with similar pattern can be observed on the bottom of ponds or aquariums after the legs of water-walking insects deform the water surface caused by the legs of water-walking insects (Andersen, 1976). Using this phenomenon, Zheng et al. (2016) devised a convenient method for empirically measuring the normal forces on the legs. The researchers found that the topography of the dimples can be significantly reflected in the size of shadows (Yin et al., 2016). There is also a significant linear relationship between the total shadow area and the total load on the legs (Zheng et al., 2016). It provides a method to estimate the vertical forces acting on the legs for tiny water-walking animals with the least possible error (Ma et al., 2020). Further, it can be utilized to precisely determine the vertical pressures during motion along with changes in the movement of the legs (Lu et al., 2018). In previous studies, however, the measurements had been restricted to actual data for a group of medium-size water striders. To assess the efficiency of bodyweight distribution in gerridaes, it is necessary to compare this characteristic across a wide range of species.

Over decades, researchers have provided extensive details regarding sculling, but the biomechanics underlying the kinematics of legs has not been fully understood in terms of load-bearing by the legs. Here, we visualized a pattern of load exerted on the legs of water striders at the standstill posture. Furthermore, we have described the functional role of each leg, as well as determined the leg movements with alternations of load value at various positions in the context of striding behavior that is characterized by a variety of features among water striders. This study predicts that the procedure for redistribution of load on the legs is a key factor that influences floating of the body and efficiency of locomotion on the elastic film of surface tension.

This project may assist in understanding the constraints in engineering water-walking machines with realistic size and shape.

Material and methods

Animals

Water striders, *Gerris argentatus*, were collected from a pond located in the Botanical Garden of Kiel University. Each experiment was carried out on more than 5 individuals (one movement/stride per individual). All procedures in this study are conducted in accordance with the ethical guidelines of Kiel University, Germany.

The total shadow area for 17 individuals with a body mass between 4 and 11 mg was measured (Fig. 2a). Upon placing the steel sinkers in the middle of dorsal side of the thorax, the body mass of two individuals was increased from 9.2 and 9.4 mg to 16.4 and 20.3 mg, respectively (Table 1, Fig. S1). The shadow area measurements were converted into percentages to facilitate easy implementation of the protocol. This simplified procedure enables us to compare weight-spreading patterns at different body postures in mature and immature water striders from diverse specimens with substantial variability in weight and size.

Table 1 The relationship between the weight of individuals and the total size of shadows caused by the distortion of the water surface

No.	Body mass (mg)	Shadow area (mm^2)
1	4.7	4.1
2	4.0	3.9
3	5.0	4.7
4	7.9	7.5
5	10.0	6.2
6	8.3	8.6
7	5.2	4.1
8	9.4	6.6
9	6.5	5.9
10	11.2	7.3
11	9.2	6.4
12	10.8	7.6
13	10.2	6.4
14	4.4	4.6
15	8.7	6.0
16	16.4*	10.9
17	20.3*	14.5

(*) individuals with extra weights on the dorsal side of the thorax.

Experimental setup

Individuals were tested in a 3D printed cubic vessel with the dimensions of $10 \times 5 \times 5$ cm (L $\times$ W $\times$ H), at room temperature (25°C; Fig. 1a). A thin glass was added at the bottom. For an accurate vision, a glass (3 mm thickness) was silanized by using a protocol for silanizing glassware (Seed, 1998), and it was added to the front of the vessel, to minimize the meniscus effect. A light source (Storz Techno Light 270 Cold Light Projector) was used above (70 cm) the vessel. The aquarium bottom was coated with a 125-micron laminating pouch (GBC), which allowed the shadows to be seen from below. The vessel was filled with distilled water of approximately 5 mm in height. The shallow depth of the water enabled us to detect contact areas between the legs and water. It also reduced the influence of the interfering waves during locomotion (Moisy et al., 2009; Steinmann et al., 2018). A mirror was placed below the screen at a 45-degree angle to capture the shadow images (1280×1024 pixels) by using a high-speed camera with 2000fps (Olympus I-Speed 3 Series High-Speed Cameras). The camera was placed 20 cm from the mirror. Before every record, water striders were weighed separately (AG204 Delta Range Analytical Balance).

Analyses procedure

The footages were analyzed by using the image analysis program ImageJ, to measure the shadow areas (Schneider et al., 2012). Each shadow area was treated as a measure of load on the leg from which that shadow originated. By converting the measurements into percentages, the per cent distribution of the total was calculated. The percentage of load on each leg was evaluated and expressed as a fraction of the body mass. The linear regression analysis was used to measure the
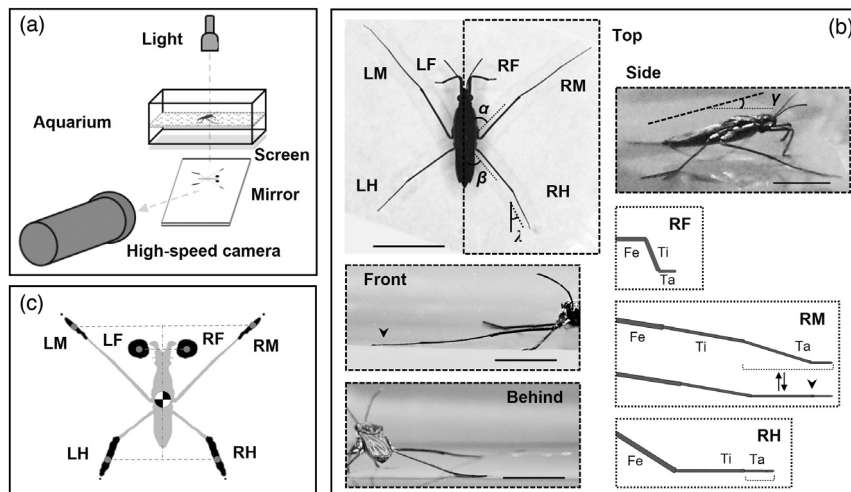
Fig. 1 Body posture of *Gerris argentatus* on the water surface. (a) Experimental setup. (b) The water strider body with the top, side, front, and behind views with some details of the right legs. From the top view, α and β show the angles between the femur of midlegs and hindlegs relative to the body centerline, respectively. λ indicates the angle between the tarsus-tibia section of hindleg relative to the body centerline, respectively. γ shows the body angle relative to the horizontal line from the side view. The schematic images of a foreleg, midleg, and hindleg (insets) from the side view. RM inset shows the midleg between two positions: when the terminal portion (top) or the whole of tarsus (bottom) is in contact with the water surface, the two-way arrow shows the transition between two positions. The arrowheads indicate the joint between two portions of the midleg tarsus. Fe, femur; Ti, tibia; Ta, tarsus. (c) Shadows below the legs. LF, LM, and LH represent the left legs, and RF, RM, and RH represent the right legs. The dark gray spots and dashed lines indicate the mid-points of shadows and their distance from the body centerline shown by the gray dashed-dotted line. The symbol indicates the body center. Scale bar: 5 mm.

correlation between the total shadow area and mass (Fig. 2a). By using the Manual-Tracking plug-in in ImageJ, displacement of the body center and legs was measured by tracking the shadows. The statistical analysis was conducted utilizing SigmaPlot 12.0 (Systat Software Inc., San José, CA, USA). Two sets of data were compared by using the *t*-test.

Glossary

Striding is a form of locomotion of water striders on the water surface by means of midleg (scull-legs), while sliding on the forelegs and hindlegs (ski-legs; Fig. 4a–d). *Sculling* is the technique for starting horizontal momentum by simultaneous using the midlegs to generate the sculling stroke, during the driving phase (when the midlegs travel backward from the catch position to the finish position and exert propulsion force on the water). *Catch position* represents the initial place of the contact part of the scull-legs when they are extended onto the water toward the anterior part of the body. *Finish position* is when the tip of each midleg moves backward, and it is raised to swing through the air after the sculling stroke has been completed. The recovery phase starts with swing of the midlegs from the finish position to the recovery position while the body continues sliding. *Recovery position* refers to the place at which the tips of the midlegs are repositioned on water following a sculling stroke. *Passive sliding* is the motion in which the body slides passively without movement of the midlegs in order to generate the sculling stroke. *Stop phase* refers to the

finishing of passive sliding while the body returns to the stand-still posture.

Symbols used

The pairs of forelegs, midlegs, and hindlegs are indicated by FL, ML, and HL, respectively (Fig. 1c). The shadows are shown by LF, LM, and LH for the left legs and RF, RM, and RH for the right legs (Pearson & Franklin, 1984).

Results

Posture assessment and weight distribution

General posture of water striders is 6-legged stance with symmetrical sprawling of leg pairs. The midlegs and hindlegs are adjusted with angles of about $\alpha = 56 \pm 2$ and $\beta = 54 \pm 2$ degrees between their femur and the body centerline, respectively. Angle of the tarsus-tibia part of the hindleg with respect to the body centerline is equal to $\lambda = 13 \pm 1$ degrees. The head is elevated above the horizontal line with an angle of about $\gamma = 15 \pm 2$ degrees (Fig. 1b).

Insect legs are composed of the coxa, trochanter, femur, tibia, and tarsus segments (Richards & Davies, 1977). Assessing various postures, we considered the tarsus, terminal of tarsus, and tarsus-tibia as load-bearing parts on the forelegs, midlegs, and hindlegs, respectively (Fig. 1b). The hindleg tarsus-tibia is approximately 6 times longer than the foreleg
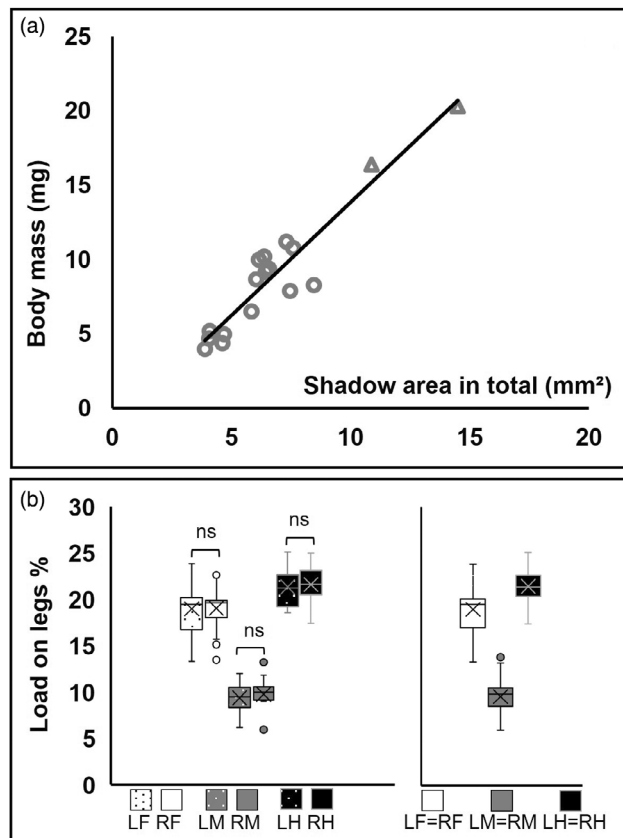
Fig. 2 Load distribution on the legs of *Gerris argentatus* at the 6-legged stand position. (a) The relationship between the body mass (mg) and the total shadow area (mm²), each circle represents the data from an individual. Two individuals with extra weight on the dorsal side of the thorax are shown by triangles. The regression line: $Y = 1.5197 X - 1.3259$, $R^2 = 0.892$, $P < 0.05$. (b) The load distribution on each single leg (left) and the average load on a single leg of each leg pair (right). In the structure of each boxplot, the × mark indicates the mean, and the horizontal line is the median, the upper and lower box edges are the upper quartile and lower quartile, respectively, the whiskers show higher and lower values, and the outside circles are outliers. "NS" indicates no significant differences ($P < 0.05$; t-test). Shadows below the forelegs, midlegs, and hindlegs are labeled as LF, LM, and LH on the left side and RF, RM, and RH on the right side, respectively. $N = 17$ individuals, each tested once.

tarsus. Also, our observations indicated that the entire midleg tarsus is frequently used to support the bodyweight.

The dark spots on the aquarium bottom in which water striders were tested show a variety of shapes including circular spots for the forelegs, whereas those for the midlegs and hindlegs were elongated with small spot at the tip related to the claws (Fig. 1c). A significant linear relationship was found between the total shadow area and the body mass (Body mass = 1.5197 × shadow area − 1.3259, $R^2 = 0.892$, $p < 0.05$; Fig. 2a). Accordingly, our linear regression analysis suggested a procedure to predict load changes in a reliable way. This equation was later used to estimate loads in Newton

units for a given shadow area (Fig. 6a). Load percentages carried on legs were LF = 19 ± 2.9%, LM = 9.4 ± 1.7%, LH = 21.3 ± 1.9%, RF = 19 ± 2.6%, RM = 9.8 ± 2.1%, and RH = 21.6 ± 1.9% of the total weight. There was no statistically significant difference between loads on the legs of each pair (t-test, $P < 0.05$; Fig. 2b left). Therefore, we have determined that the proportional weight distribution on the legs at standstill posture is as follows: LF ≈ RF ≈ 19%, LM ≈ RM ≈ 10%, LH ≈ RH ≈ 21% of the total (Fig. 2b right).

Weight distribution changes when forelegs are off water

In some cases, water striders switch their stance from 6-legged to 4-legged posture by raising the forelegs, that is, without change in the adjustment of other legs (Fig. 3a–c, Video S1). In 4-legged stance, loads on the legs were LM = 25.3 ± 3.7%, RM = 26.7 ± 1.7%, LH = 24.3 ± 2.6%, and RH = 23.7 ± 1.9%. Thus, loads carried by the leg pairs were ML ≈ 52% and HL ≈ 48% of the total (Fig. 3d, e). Considering that the duration of switching from 6-legged to 4-legged posture differed depending upon the individual, we extracted 10 frames from every performance. We also measured the change in load on each pair, which is ascending for both midlegs and hindlegs (Fig. 3e). Load shifting occurred nonstationary from FL to ML and HL in an order of 86% and 14%, respectively (Fig. 3e, insets). Load shifting happens at a higher value in the beginning and then gradually continues until the forelegs detach from water.

Comparison of the total load on the legs between 6-legged and 4-legged stances showed no significant difference, further demonstrating the validity of the method employed here (Fig. S2).

Stride performance

The stride cycle was assessed while individuals exhibit straightforward locomotion with symmetric sculling, i.e., when difference of α on two sides was ≤10° during the corresponding midlegs kinematics (Fig. 4a, c; Video S2). Otherwise, asymmetrical widening of the midlegs leads to progressive deviation from the straight trajectory of locomotion. Each scull-leg tip travels on water through an arc, then swings to the recovery position that follows an S-shaped trajectory (Fig. 4b). This mechanism is different from the oar blade movement through water during the driving of sculling boats (Caplan et al., 2010; Coker, 2010; Feigean et al., 2017). Trajectories of the ski-legs look like straight lines; however, the forelegs frequently display adduction and abduction to the body axis (Fig. 4a, b). Furthermore, there was an increase in the distance between the mid-point of foreleg shadows to the body center during sculling and early of passive sliding.

The body shows a short-term upward movement during the driving phase that is synchronized with flexion of the forelegs at the coxa–femur and femur–tibia joints (Fig. 4a). The forelegs show a quick angular movement at the coxa–femur joints during the body downward movement, although the femur–tibia joints remained flexed position for a longer time.
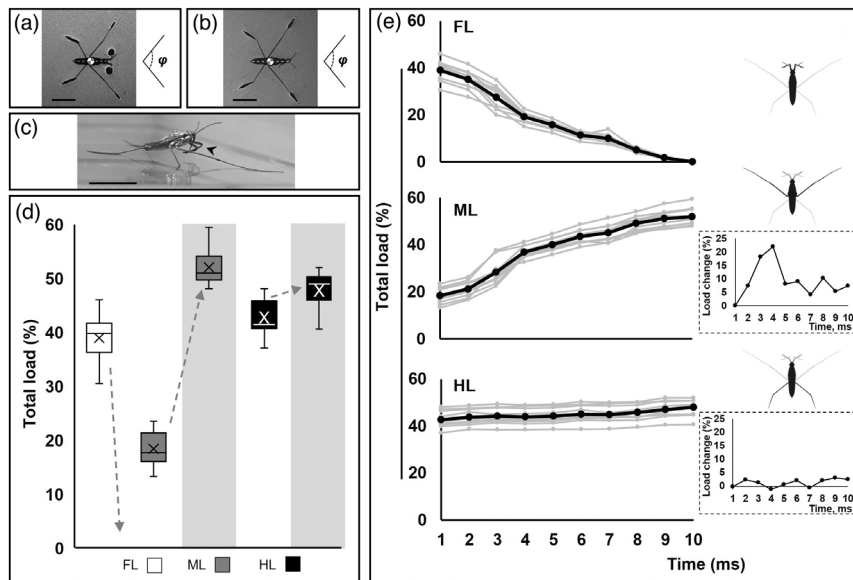
Fig. 3 Switching of the body position from 6-legged to 4-legged stance. (a and b) In both postures, φ is the angle between the midleg femurs. There is no significant differences for φ between two postures ($P < 0.05$; t-test). (a) The shadow of body at 6-legged stance position. (b) The shadow of body at 4-legged stance position. (c) The side view, arrowhead indicates the raised forelegs. (d) Load changes on the leg pairs after the switch from 6-legged to 4-legged stance (shown by gray columns in the background). In the structure of each boxplot, the × mark indicates the mean, and the horizontal line is the median, the upper and lower box edges are the upper quartile and lower quartile, respectively, the whiskers show higher and lower values. (e) Changes of the load on the leg pairs during raising the foreleg pair. The insets show the instant load gaining rate on the midleg and hindleg pairs. FL, ML, and HL represent the pair of forelegs, midlegs, and hindlegs, respectively. $N = 10$ individuals, each tested once. Scale bar: 5 mm.

As locomotion begins, the legs undergo angle changes with respect to the body axis (Fig. 4c). The midlegs drive over an angle of ≈66 ± 3 degrees with the highest angular velocity of ≈19 rad/s. We measured the body velocity and the traveling distance as well as the body momentum with velocity and acceleration of the midlegs for five individuals (Fig. 4e–g). Also, the averages of velocities and accelerations of the midlegs were measured for each individual (Fig. 4f). In correlation with increasing velocity of the midlegs, the body velocity rapidly increased during the driving phase to the highest point, then gradually decreased toward zero during the recovery phase (Fig. 4e, f). Maximum velocities, sculling durations, traveling distances, and stride durations were in the range of 0.16–0.24 mm/ms, 75–90 ms, 33–44 mm, and 705–735 ms, respectively (Table 2).

During early sculling, the tarsus-tibia parts of the hindlegs, in combination with the slight flexion of the hindlegs at the coxa–femur joints, rotate inward in relation to the femur to form the parallel skiing position respect to the centerline. Ski position of the hindlegs remains fixed until the end of swing stage, afterward all the legs gradually return to the starting position by the end of locomotion (Fig. 4a, b). In the parallel position, the mid-point of the hindleg shadows of two sides are closer to each other and to the body center than the standing posture. During the release stage, the midlegs move backward and upward with a slight bending inward along the tips detached from water (Fig. 4a). During recovery phase, the

midlegs swing through the air over an angle of $θ ≈ 78 ± 2$ degrees. The midlegs gently spread apart after lying down on water; likewise, the body adjustment continues with re-angulation of all the leg joints akin to the starting posture (Fig. 4a–d).

Loading and unloading of legs during sculling

During a specified period (285 ms), loads on the legs were measured and plotted for each leg (Fig. 5a, Video S3). Load changes on the legs occurred instantly when starting sculling. Despite some variations between individuals, the mean curves of the legs of each pair show synchronicity (Fig. 5a). While the load on the midlegs reached a peak, those on the forelegs and hindlegs dropped below the baselines, although all graphs remained above zero. Load on the forelegs increased dramatically during the swing stage, while it changed on the hindlegs to a small hump. During recovery phase, load on each foreleg decreased toward the baseline, whereas the graphs of the hindlegs remained with a low range of changes. However, the ascending trends of the forelegs and hindlegs graphs show fluctuations with small up-down changes (Fig. 5b). Load on the midlegs increased as soon as their tips lay down on water (Fig. 5a).

By using the regression analysis equation, load changes were calculated in total and on the scull-legs for individuals
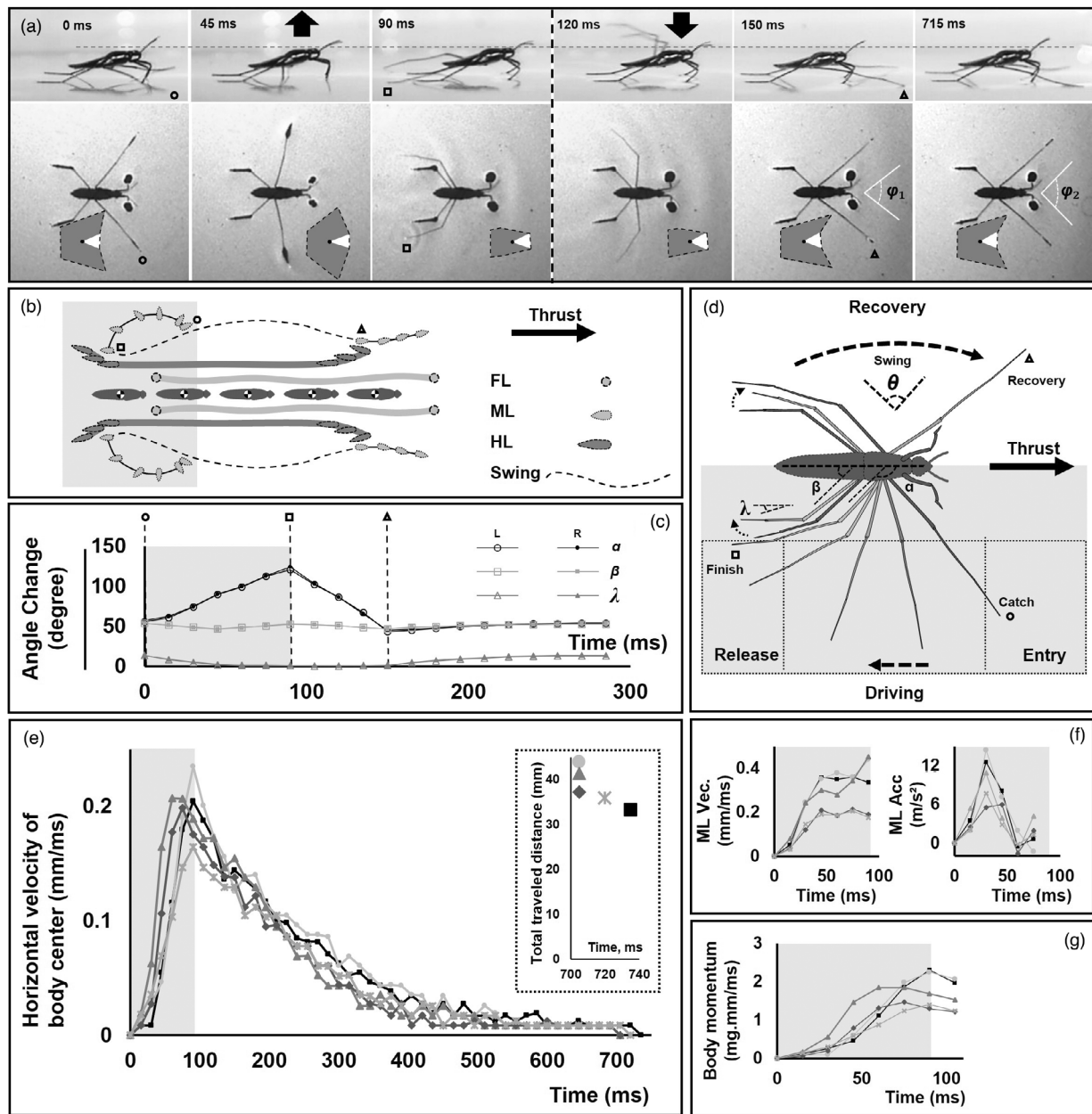
Fig. 4 Leg kinematics during striding. (a–d) The circle, square, and triangle indicate three key positions of midlegs at the catch, finish, and recovery positions, respectively. (a) Sequences of a striding cycle in the side view and from the bottom. Vertical dashed line separates the driving phase (left) and the recovery phase (right). Surrounded areas by black dashed lines indicate the base of support for each body posture (areas are minimized), the black dots indicate the body center. White triangles indicate the fraction of each area that is affected by movement of the forelegs. The arrows indicate upward and downward movements of the body. Horizontal dashed line is the indicator to detect the upward and downward movement of the body. φ_1 and φ_2 are the angles between the midleg femurs at the recovery position and after stopping, $\varphi_2 \geq \varphi_1$. (b–g) The gray boxes in the background indicate the driving phase. (b) A schematic diagram shows the motion traces of the body center, foreleg tarsi (gray circles), midleg tips (gray plain shapes and black lines/dashed lines), tarsus-tibia parts of the hindleg (dark gray plain shapes) during striding. The dashed curve black lines indicate swing trajectories of the midleg tips. (c) Changes in angles between the femur of midlegs α, the femur of hindlegs β, and the tarsus-tibia part of hindleg λ with respect to the body centerline, L and R indicate lift and right sides, respectively. (d) The midleg movement during the driving phase is depicted by a gradient of darkness, the dashed arrows show the direction of leg movement. θ and the dashed curve arrow represent the swing angle and the direction of midleg movement from the finish position to the recovery position. The dotted curve arrows behind the hindleg represent the movement direction of the contact area during striding. (e) The body velocity versus time. The inset indicates the total traveled distances. (f) The velocity (left) and acceleration (right) of midlegs that are indicated by ML Vec. and ML Acc., respectively. (g) The body momentum versus time. $N = 5$ individuals, each tested once.

with a body mass between 5.7 and 11.0 mg (on average 8.5 mg; Table 3). The mean total load showed a sudden increase during the driving phase and then gradually declined during the recovery phase (Fig. 6a). Difference between the total load in motion and that in the static state was termed *dynamic load*, which represents the additional loads generated by the insects (Fig. 6a, b). Based on the average graphs, the maximum *dynamic load* and the load difference on the scull-legs were about ~35 and ~ 41 μN, respectively.

Discussion

The leg adjustment of water striders at the standstill posture

Weight spreading of a living body correlates with the spatio-temporal configuration of load-bearing parts such as the legs (Isakov et al., 1992; Laufer et al., 2000). There appears to be a correlation between the leg morphology of water striders and their floating ability and motion (Crumiere et al., 2016; Liu et al., 2007; Zhao et al., 2022). The long legs facilitate weight spreading that allows them to stand on water (Goodwyn et al., 2008; Hu et al., 2003). In addition to proportional adjustment, the flexibility of the legs is critical to improving float ability (Ji et al., 2012; Koh et al., 2015; Wei et al., 2009;

Table 2 Velocity, traveling distance, and duration of rowing measurements

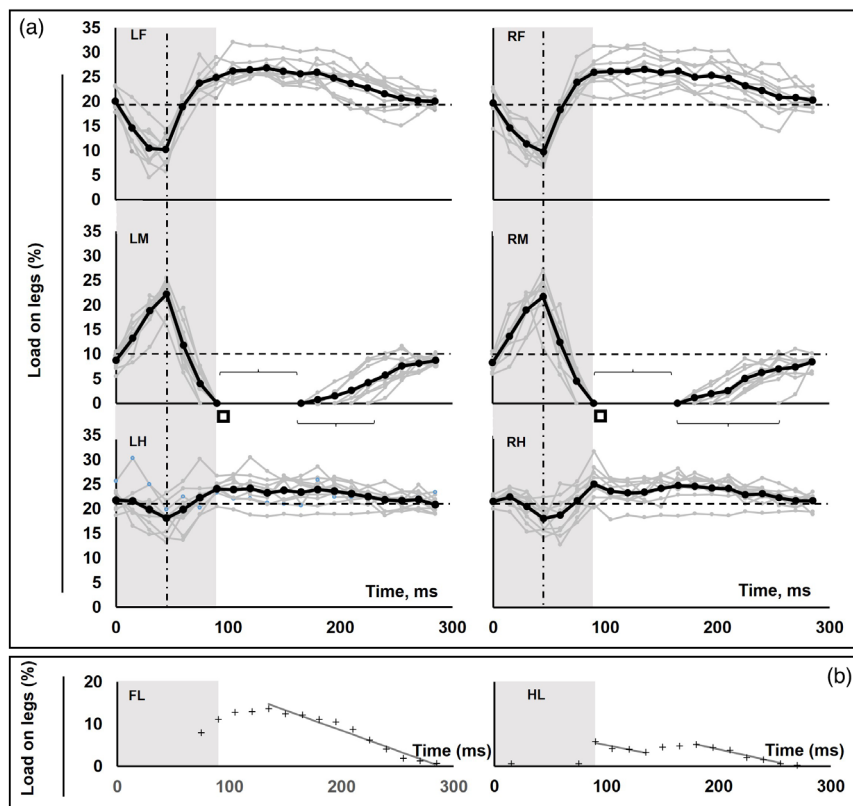| No.	Body mass (mg)	Velocity (mm/ms)	Traveled distance (mm)	Duration of sculling stroke (ms)	Duration of striding (ms)
1	9.4	0.20	33.1	75	735
2	9.6	0.24	43.9	75	705
3	10.3	0.21	41.3	90	705
4	11.0	0.20	37.2	90	705
5	8.9	0.16	35.9	75	720

Fig. 5 Kinetics of sculling. (a and b) The gray boxes in the background indicate the driving phase. (a) The gray lines indicate the patterns of load distribution on the legs of individuals, and the black lines represent the averages. The discrete points represent the time of frames, extracted from the high-speed recorded footages. Empty squares indicate the finish position. Horizontal dashed lines are the baseline of load average on the legs during the starting position. The downward brackets indicate the average swing duration, and the upward brackets indicate the times at which the midlegs were reattached to the water surface. The vertical dashed-dotted lines indicate when maximum loads are exerted on the mid-legs. (b) Differences of load changes on the foreleg and hindleg pairs. The black lines are regression lines for the descending load changes on the leg pairs. Shadows below the forelegs, midlegs, and hindlegs are labeled as LF, LM, and LH on the left side and RF, RM and RH on the right side, respectively. FL and HL represent the pair of forelegs, midlegs, and hindlegs respectively. *N* = 10 individuals, each tested once.

Table 3 Maximum of dynamic load and load on the midlegs measurements

No.	Body mass (mg)	Max. dynamic load (μN)	Max. load differences on the midlegs (μN)
1	9.8	35	49
2	10.5	37	55
3	10.3	43	52
4	11	46	58
5	8.9	36	37
6	7.5	32	34
7	7.3	42	51
8	6.7	45	59
9	6.9	27	36
10	5.7	25	31

Zheng et al., 2009). In semi-aquatic insects, the flexibility of the legs enables them to conform to the water surface for effective body support (Kong et al., 2015). Morphological differences in part of the legs that interact with the water surface result in a variety of shadow sizes and shapes, but their combination is sufficient for the bodyweight bearing (Zheng et al., 2016). It is expected that a balanced floating body will result from a proportional load distribution on the legs. The bodyweight is predominantly distributed on the hindlegs and forelegs (Fig. 2b). However, in contrast to the hindlegs, the forelegs have a shorter length of contact area with the water surface. It shows that a higher value of load can be supported by each unit of the foreleg than the midlegs or hindleg, suggesting that maybe the forelegs can support higher load or, that for some reason, water striders put more load on them. If the former is the case, then it hypothetically suggests that the

structure, density, and arrangement of hairs on the forelegs may provide a high capacity to support loads.

The values of angles describing the leg positions (Fig. 1b, upper left) combined with quantification of load supported on the legs (Fig. 2b) can contribute to understanding of the body-weight distribution during 6-legged stance posture of water striders. Although the size of studied water striders is considerably different, there is a high similarity in the load distribution pattern on the legs based on percentage between our research and the former study by Lu et al. (2018). Based on these results, there may be an optimal load distribution for water striders; however, this can be more accurately determined by assessment of water striders with different sizes.

Water striders begin sculling from a particular initial leg adjustment and return to it at the end of locomotion (Lu et al., 2018; Fig. 1b). Regardless of their movement (sculling, raising the legs, grooming, etc.), the body postures always return to the pattern outlined earlier that we consider it as the starting posture. It differs from rest posture when they attach themselves to floating objects and walls (Keiser, 2016; Fig. S3).

Changes in load distribution between 6- and 4-legged stance

Water striders raise their legs to groom, apply hydrophobic substances to the skin, or grab foods (Mahadik et al., 2020; Staddon, 1972; Zheng et al., 2016). Despite the absence of support on one or two legs, the floating body remains stable due to redistribution of the bodyweight. However, we never observed water striders raising more than two legs at the same time.
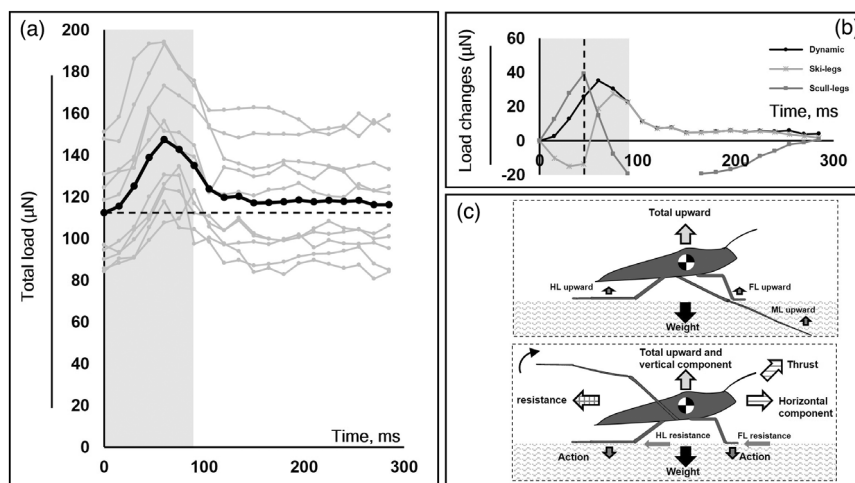

Fig. 6 Load components on the legs at the dynamic state. (a and b) The gray boxes in the background indicate the driving phase. (a) The black line is the average value of total load, and the gray lines represent data obtained from each individual. The dashed line indicates the average total load at the starting posture. (b) Differences in load changes on the scull-legs (midlegs), the ski-legs (both forelegs and hindlegs) and dynamic load shown by the gray, faint gray and black lines, respectively. The gap in the line of scull-legs indicates the duration of swing. Vertical dashed line indicates the approximate time of upward movement of the body. (c) Forces acting on the body of water striders during standing (Top) and striding (Bottom). $N = 10$ individuals, each tested once.

The usual behavior of water striders is to switch from 6-legged to 4-legged stance by raising both the forelegs simultaneously (Fig. 3a–c). Gradual load shifting from the forelegs may assist with conformity of the legs with the water surface, as well as body alignment to the new posture (Fig. 3e, insets). The midlegs, for instance, can support a substantial percentage of bodyweight by utilizing the entire tarsus (Fig. 1b). But it is only the terminal part of the midleg tarsus that is in contact with the water during sculling, thus facilitating its release from the surface (Gao & Feng, 2011). During a critical state, the midlegs may play a crucial compensatory role by gaining additional loads to prevent immersion of the floating body.

Spatial configuration of the legs as an essential factor in sculling

The typical sculling consists of a set of bilateral movements of the midlegs (Darnhofer-Demar, 1968). As a contrast, when water striders carry prey bodies by using their forelegs, they demonstrate asymmetrical sculling, with one midleg supporting the body and the other performing driving (Kim et al., 2022). During the sculling stroke, water striders transfer momentum to the subsurface water principally through hemispherical vortices while the midlegs and menisci beneath them work as oars and blades, respectively (Bühler, 2007; Hu et al., 2003; Hu & Bush, 2010). The midlegs demonstrate a wide range of configurations in all the joints to place from the catch to driving and release positions in order to impart momentum (Fig. 4a–d).

Water striders stand on six points of contact, while the body center is located over the middle of the base of support (Fig. 4a). The base of support refers to the area beneath the body and within the points where the legs contact the surface (Binder et al., 2008). A larger base of support that is obtained by widening angle of the legs improves the body posture during stepping (Gruhn et al., 2008; Merienne et al., 2020). In this regard, movements of the forelegs to the sides can contribute to improving floating of the body while the slide trajectory stays straightforward (Fig. 4a). Although changes in the angle of hindlegs are not intense, position changing of the hindleg tarsus-tibia parts from spreading apart to parallel may assist in sliding. As reported before, the hindlegs can be used as rudders for motion trajectory (Andersen, 1976; Pratt, 1938; Tseng & Rowe, 1999), but it is unclear whether the hindlegs are functionally independent of the other legs. Thus, striding is regarded as a dynamic activity with the assistance of all legs. A stride cycle is ended with readjustment of the legs to the starting posture that puts the body on standby position. The starting posture appears to be necessary for immediate motion and may reduce the risk of sculling failure.

Dynamical analyses during a full stride performance

The body velocity is an important quantity that provides a clear view of the interaction between propelling and sliding. Despite the similar sizes, their stride performances were characterized by distinctive features in terms of traveling times and lengths (Fig. 4e). The acceleration magnitude of the midlegs seems to be correlated with the initial body movement, although other parameters such as configuration of the legs, resistance, and morphological differences can lead to variations in the body velocities (Fig. 4f). The midlegs are moved in both the horizontal and vertical directions during the driving phase (Wei et al., 2009). Water striders intensify their leg force progressively in order to increase imparting momentum to the fluid (Koh et al., 2015). As a result of flexibility of the legs, the midlegs can push the water down deeper without breaking the surface tension (Steinmann et al., 2021; Yan et al., 2018). Due to stronger stroke, higher propulsion power is produced during sculling (Gao & Feng, 2011). Although there is constraint for measuring spatial movement of legs, velocity of the midlegs and the body momentum exhibit high coincidence (Fig. 4f, g). Changes in vertical load that happen coincide with acceleration of the midlegs that might enhance the transfer of forces to legs to propel themselves as quickly as possible without breaking the interface. Upon the midlegs are released from water, the bodies achieve the maximum momentum.

The individuals with higher initial velocities may travel further distances, but not for the longest time. The individuals with lower initial velocities established a variety of strides, which indicates no strong correlation between initial velocity, length of traveled distance, and sliding duration. This implies that water striders control their locomotion behavior at the propelling and sliding levels in order to reach a particular destination.

Load changes during the sculling performance

The legs must be loaded symmetrically during the straightforward striding while the legs show extensive alteration at the joints (Figs 4c, 5a). With changes in the leg adjustment, water striders sustain floating by load shifting among their legs (Yin et al., 2016; Zheng et al., 2016). The legs are predicted to exchange loads repeatedly to maintain the body stable. The initial surge of pressure on the forelegs with a subsequent load reduction on the hindlegs indicates that the body is anteriorly tilted after sculling. The body begins to gently lean backward and loads shift toward the posterior, while the total load curve descends to the baseline (Fig. 6a). As loads on the ski-legs decrease during the recovery phase, the trends show a relatively low range of fluctuations (Fig. 5b). Possibly, the fluctuations represent action of the forelegs and hindlegs in producing pressure on the water surface to assist with stabilizing of the body. It may lead to an idea that the function of ski-legs is expanded from a weight supporter to a stabilizer (Figs 5b, 6c).

During the driving phase, load on the scull-legs reaches a peak while the ski-legs begin to lose load (Fig. 5a). A decrease in load on the forelegs can be attributed to flexion of the joints and the body upward movement (Fig. 4a). It may lead to lower resistance between the forelegs and the water surface, and water striders achieve a greater initial thrust. A load peak on the midlegs is caused by propelling with an additional load in the absence of support from the forelegs (Fig. 6b). In other

words, the maximum load on the midlegs is the sum of their vertical pressure and the shifted weight from the ski-legs. In contrast to the oar blades entering the water, vertical pressure is required for the midlegs to effectively push the water beneath backward, which is believed to be necessary for sculling. A vertical pressure changes in depth of minuscus below to the tip and affects the amount of vortex in the flow (Steinmann et al., 2021).

At two distinct times, the loads on the ski-legs and scull-legs reach the maximum levels (Fig. 6b). With the contribution of all the legs, *dynamic load* steadily increases to reach the maximum point at a time between the two peaks. As the driving phase is being completed, a high value of load shifts on the ski-legs. The forelegs appear to be adapted to gain a substantial value of extra load during the swing stage, but the hindlegs act to smoothly spread it during the recovery phase (Figs 5a, b, 6b). As the midlegs are reattached to water, loads on the legs tend to be directed toward the baseline during the recovery phase to establish the starting posture. Thus, the scull-legs and ski-legs can compensate each other to prevent load disproportional variations. In consequence, the smooth load redistribution occurs on the legs while it is associated with the gentle sliding on the water surface.

This study can contribute to understanding of the freedom degree of joints and other effective parameters in striding of water striders. It can provide a link between behavioral studies and adaptation of water striders to exhibit a variety of locomotions. It may lead to the design water-walking machines with high floating ability to exhibit long-term locomotion.

Conclusions

Configuration of legs and load distribution in the water strider *Gerris argentatus* were studied in both static and dynamic states. Water striders adjust their legs to achieve a standstill body posture while the bodyweight is distributed on each single foreleg, midleg, and hindleg in order of 19%, 10%, and 21% of the total, respectively.

Striding behavior is associated with a wide variety of characteristics, which are controlled by water striders. On average, individuals with ~10 mg mass can reach the peak velocity of ~0.20 mm/ms and proceed ~38 mm distance in 715 ms. Although the midlegs are responsible for froward propulsion, the forelegs and hindlegs actively contribute to striding throughout the locomotion. In addition to moving the midlegs quickly horizontally, the tip of the midlegs seems to press the surface vertically. Smooth load shifting among the legs in conjunction with a particular configuration of legs allows water striders to achieve gentle locomotion on the water surface. The results can be used to better understand leg kinematics by which water striders maintain floating and slide on water. It can also help to improve layouts design of water-skating robots through their locomotion. Through this study, it will be possible to discuss not only how the forelegs and hindlegs are used for supporting the body but also how they assist in striding by modifying the body posture. However, the principal mechanism of load alteration remains a matter of debate that will be discussed in the future.

Conflict of interests

The authors declare there are no conflicts of interest to disclose.

References

Andersen, N. M. (1976). A comparative study of locomotion on the water surface in semiaquatic bugs (Insects, Hemiptera, Gerromorpha). *Videnskabelige Meddelelser fra Dansk Naturhistorisk Forening*, **139**, 337–396.

Andersen, N. M. (1982). *The semiaquatic bugs (Hemiptera: Gerromorpha). Phylogeny, adaptations, biogeography, and classification*. Scandinavian Science Press.

Baek, M., Lawin, K. M., Codden, C. J., Lim, H., Yang, E., Kim, H., Lee, S., & Jablonski, P. G. (2020). Water strider females use individual experience to adjust jumping behavior to their weight within physical constraints of water surface tension. *Scientific Reports*, **10**(18), 657. https://doi.org/10.1038/s41598-020-75564-x

Binder, M. D., Hirokawa, N., & Windhorst, U. (2008). *Base of support (BOS), Encyclopedia of neuroscience*. Springer. https://doi.org/10.1007/978-3-540-29678-2_568

Bühler, O. (2007). Impulsive fluid forcing and water strider locomotion. *Journal of Fluid Mechanics*, **573**, 211–236. https://doi.org/10.1017/S002211200600379X

Bush, J. W. M., Hu, D., & Prakash, M. (2007). The integument of water-walking arthropods: Form and function. *Advances in Insect Physiology*, **34**, 117–192. https://doi.org/10.1016/S0065-2806(07)34003-4

Bush, J. W. M., & Hu, D. L. (2006). Walking on water: Biolocomotion at the interface. *Annual Review of Fluid Mechanics*, **38**(1), 339–369. https://doi.org/10.1146/annurev.fluid.38.050304.092157

Caplan, N., Coppel, A., & Gardner, T. (2010). A review of propulsive mechanisms in rowing. *Proceedings of the Institution of Mechanical Engineers, Part P: Journal of Sports Engineering and Technology*, **224**(1), 1–8. https://doi.org/10.1243/17543371JSET38

Caponigro, M. A., & Eriksen, C. H. (1976). Surface film locomotion by the water strider, *Gerris remigis* Say. *American*

Midland Naturalist, **95**(2), 268–278. https://doi.org/10.2307/2424392

Coker, J. (2010). Using a Boat Instrumentation System to Measure and Improve Elite On-Water Sculling Performance. Doctoral dissertation, Auckland University of Technology, Auckland. http://hdl.handle.net/10292/995

Crumiere, A. J. J., Santos, M. E., Sémon, M., Armisén, D., Moreira, F. F. F., & Khila, A. (2016). Diversity in morphology and locomotory behavior is associated with niche expansion in the semi-aquatic bugs. *Current Biology*, **26**(24), 3336–3342. https://doi.org/10.1016/j.cub.2016.09.061

Darnhofer-Demar, B. (1968). The locomotion of the pond skater *Gerris lacustris* L. on the water surface. *Verhandlungen der Deutschen Zoologischen Gesellschaft*, **28**, 430–439. US201301175204.

Denny, M. W. (2004). Paradox lost: Answers and questions about walking on water. *Journal of Experimental Biology*, **207**(10), 1601–1606. https://doi.org/10.1242/jeb.00908

Feigean, M., R'Kiouak, M., Bootsma, R. J., & Bourbousson, J. (2017). Effects of intensive crew training on individual and collective characteristics of oar movement in rowing as a coxless pair. *Frontiers in Psychology*, **8**, 1139. https://doi.org/10.3389/fpsyg.2017.01139

Feng, X., Gao, X., Wu, Z., Jiang, L., & Zheng, Q. (2007). Superior water repellency of water strider legs with hierarchical structures: Experiments and analysis. *Langmuir*, **23**(9), 4892–4896. https://doi.org/10.1021/la063039b

Gao, P., & Feng, J. (2011). A numerical investigation of the propulsion of water walkers. *Journal of Fluid Mechanics*, **668**, 363–383. https://doi.org/10.1017/s0022112010004763

Gao, X., & Jiang, L. (2004). Water-repellent legs of water striders. *Nature*, **432**, 36. https://doi.org/10.1038/432036a

Goodwyn, P. P., Wang, J., Wang, Z., Ji, A., Dai, Z., & Fujisaki, K. (2008). Water striders: The biomechanics of water locomotion and functional morphology of the hydrophobic surface (Insecta: Hemiptera-Heteroptera). *Journal of Bionic Engineering*, **5**(2), 121–126. https://doi.org/10.1016/s1672-6529(08)60015-3

Gruhn, M., Zehl, L., & Buschges, A. (2008). Straight walking and turning on a slippery surface. *Journal of Experimental Biology*, **212**(2), 194–209. https://doi.org/10.1242/jeb.01831710.1242/jeb.018317

Hu, D. L., & Bush, J. W. M. (2010). The hydrodynamics of water-walking arthropods. *Journal of Fluid Mechanics*, **644**, 5–33. https://doi.org/10.1017/s0022112009992205

Hu, D. L., Chan, B., & Bush, J. W. M. (2003). The hydrodynamics of water strider locomotion. *Nature*, **424**, 663–666. https://doi.org/10.1038/nature01793

Isakov, E., Mizrahi, J., Ring, H., Susak, Z., & Hakim, N. (1992). Standing sway and weight-bearing distribution in people with below-knee amputations. *Archives of Physical Medicine and Rehabilitation*, **73**(2), 174–178.

Ji, X., Wang, J., & Feng, X. (2012). Role of flexibility in the water repellency of water strider legs: Theory and experiment. *Physical Review E*, **85**(2), 021607. https://doi.org/10.1103/PhysRevE.85.021607

Keiser, A. (2016). Water Velocity Preferences of Water Striders (Hemiptera: Gerridae) in Dominica. Keiser Department of Entomology Texas A&M University, College Station, TX.

Keller, J. B. (1998). Surface tension force on a partly submerged body. *Physics of Fluids*, **10**(11), 3009–3010. https://doi.org/10.1063/1.869820

Kiehn, R. M. (2007). *Falaco solitons-Black holes in a swimming pool*. University of Houston Copyright CSDC. Inc.

Kim, H., Amauger, J., Jeong, H., Lee, D., Yang, E., & Jablonski, P. G. (2017). Mechanics of jumping on water. *Physical Review Fluids*, **2**(100), 505. https://doi.org/10.1103/PhysRevFluids.2.100505

Kim, W., Pham, T. H., Nguyen, P. D., Tran, A. D., Ha, J., Jablonski, P. G., & Lee, S. (2022). Locomotion and flow speed preferences in natural habitats by large water striders, *Ptilomera tigrina*, with micro-morphological adaptations for rowing. *Journal of Ethology*, **40**(3), 211–221. https://doi.org/10.1007/s10164-022-00749-y

Koh, J., Yang, E., Jung, G., Jung, S., Son, J. H., Lee, S., Jablonski, P. G., Wood, R. J., Kim, H., & Cho, K. (2015). Jumping on water: Surface tension-dominated jumping of water striders and robotic insects. *Science*, **349**(6247), 517–521. https://doi.org/10.1126/science.aab1637

Kong, X. Q., Liu, J. L., Zhang, W. J., & Qu, Y. D. (2015). Load-bearing ability of the mosquito tarsus on water surfaces arising from its flexibility. *AIP Advances*, **5**, 037101. https://doi.org/10.1063/1.4908027

Krupa, J. J., & Sih, A. (1993). Experimental studies on water strider mating dynamics: Spatial variation in density and sex ratio. *Behavioral Ecology and Sociobiology*, **33**, 107–120. https://doi.org/10.1007/BF00171662

Laufer, Y., Dickstein, R., Resnik, S., & Marcovitz, E. (2000). Weight-bearing shifts of hemiparetic and healthy adults upon stepping on stairs of various heights. *Clinical Rehabilitation*, **14**(2), 125–129. https://doi.org/10.1191/026921500674231381

Liu, J. L., Feng, X. Q., & Wang, G. F. (2007). Buoyant force and sinking conditions of a hydrophobic thin rod floating on water. *Physical Review E, Statistical, Nonlinear, and Soft Matter Physics*, **76**(6 Pt 2), 066103. https://doi.org/10.1103/physreve.76.066103

Lu, H., Zheng, Y., Yin, W., Tao, D., Pesika, N., Meng, Y., & Tian, Y. (2018). Propulsion principles of water striders in sculling forward through shadow method. *Journal of Bionic Engineering*, **15**(3), 516–525. https://doi.org/10.1007/s42235-018-0042-8

Ma, J. Z., Lu, H. Y., Li, X. S., & Tian, Y. (2020). Interfacial phenomena of water striders on water surfaces: a review from biology to biomechanics. *Zoological Research*, **41**(3), 231–246. https://doi.org/10.24272/j.issn.2095-8137.2020.029

Mahadik, G. A., Hernandez-Sanchez, J. F., Arunachalam, S., Gallo, A., Jr., Cheng, L., Farinha, A. S., Thoroddsen, S. T., Mishra, H., & Duarte, C. M. (2020). Superhydrophobicity and size reduction enabled *Halobates* (Insecta: Heteroptera, Gerridae) to colonize the open ocean. *Scientific Reports*, **10**, 7785. https://doi.org/10.1038/s41598-020-64563-7

Merienne, H., Latil, G., Moretto, P., & Fourcassié, V. (2020). Walking kinematics in the polymorphic seed harvester ant *Messor barbarus*: influence of body size and load carriage. *Journal of Experimental Biology*, **223**(Pt 3), jeb205690. https://doi.org/10.1242/jeb.205690

Moisy, F., Rabaud, M., & Salsac, K. (2009). A synthetic Schlieren method for the measurement of the topography of a liquid interface. *Experiments in Fluids*, **46**, 1021. https://doi.org/10.1007/s00348-008-0608-z

Ortega-Jimenez, V. M., von Rabenau, L., & Dudley, R. (2017). Escape jumping by three age-classes of water striders from smooth, wavy and bubbling water surfaces. *Journal of Experimental Biology*, **220**, 2809–2815. https://doi.org/10.1242/jeb.157172

Pearson, K. G., & Franklin, R. (1984). Characteristics of leg movements and patterns of coordination in locusts walking on rough terrain. *The International Journal of Robotics Research*, **3**(2), 101–112. https://doi.org/10.1177/027836498400300209

Pratt, R. Y. (1938). Striding habits in the Gerridae. *Pan-Pacific Entomologist*, **14**, 157.

Richards, O. W., & Davies, R. G. (1977). *Imms' general textbook of entomology, structure, physiology and development* (Vol. **1**, pp. 46–50). Chapman and Hall Ltd. https://doi.org/10.1007/978-94-011-6514-3

Rinoshika, A. (2012). Vortical dynamics in the wake of water strider locomotion. *Journal of Visualization*, **15**(2), 145–153. https://doi.org/10.1007/s12650-011-0117-7

Schneider, C., Rasband, W., & Eliceiri, K. (2012). NIH Image to ImageJ: 25 years of image analysis. *Nature Methods*, **9**, 671–675. https://doi.org/10.1038/nmeth.2089

Seed, B. (1998). Silanizing glassware. *Current Protocols in Protein Science*, **13**(1), A.3E.1–A.3E.2. https://doi.org/10.1002/0471140864.psa03es13

Staddon, B. W. (1972). On the suggestion that the secretion from the metathoracic scent glands of a surface-dwelling aquatic insect, Gerris Najas (De Geer), (Heteroptera; Gerridae) has a waterproofing function. *The Journal of Experimental Biology*, **57**, 765–769.

Steinmann, T., Arutkin, M., Cochard, P., Raphaël, E., Casas, J., & Benzaquen, M. (2018). Unsteady wave pattern generation by water striders. *Journal of Fluid Mechanics*, **848**, 370–387. https://doi.org/10.1017/jfm.2018.365

Steinmann, T., Cribellier, A., & Casas, J. (2021). Singularity of the water strider propulsion mechanisms. *Journal of Fluid Mechanics*, **915**, A118. https://doi.org/10.1017/jfm.2021.156

Tseng, M., & Rowe, L. (1999). Sexual dimorphism and allometry in the giant water strider *Gigantometra gigas*. *Canadian Journal of Zoology*, **77**(6), 923–929. https://doi.org/10.1139/z99-071

Vinnichenko, N. A., Plaksina, Y. Y., Baranova, K. M., Pushtaev, A. V., & Uvarov, A. V. (2018). Mobility of free surface in different liquids and its influence on water striders locomotion. *Environmental Fluid Mechanics*, **18**, 1045–1056. https://doi.org/10.1007/s10652-018-9577-9

Waldbauer, G. (2006). *A walk around the pond: Insects in and over the water* (pp. 109–111). Harvard University Press.

Wei, P. J., Shen, Y. X., & Lin, J. F. (2009). Characteristics of water strider legs in hydrodynamic situations. *Langmuir*, **25** (12), 7006–7009. https://doi.org/10.1021/la900185a

Yan, J., Yang, Y., Yang, K., & Zhao, J. (2018). Study on the Rowing of Flexible Actuating Leg on Water Surface Intimating Water Striders. 2018 IEEE International Conference on Information and Automation (ICIA) (pp. 196–202). https://doi.org/10.1109/ICInfA.2018.8812533

Yang, E., Son, J. H., Lee, S., Jablonski, P. G., & Kim, H. Y. (2016). Water striders adjust leg movement speed to optimize takeoff velocity for their morphology. *Nature Communications*, **7**(13), 698. https://doi.org/10.1038/ncomms13698

Yin, W., Zheng, Y. L., Lu, H. Y., Zhang, X. J., & Tian, Y. (2016). Three-dimensional topographies of water surface dimples formed by superhydrophobic water strider legs. *Applied Physics Letters*, **109**(163), 701. https://doi.org/10.1063/1.4964788

Zhao, Y., Chu, C., Zhang, B., Lv, C., & Feng, X. Q. (2022). Experimental and theoretical studies on the dynamic landing of water striders on water. *Soft Matter*, **18**(18), 3575–3582. https://doi.org/10.1039/D2SM00208F

Zheng, Q. S., Yu, Y., & Feng, X. Q. (2009). The role of adaptive-deformation of water strider leg in its walking on water. *Journal of Adhesion Science and Technology*, **23**(3), 493–501. https://doi.org/10.1163/156856108X379155

Zheng, Y., Lu, H., Yin, W., Tao, D., Shi, L., & Tian, Y. (2016). Elegant shadow making tiny force visible for water-walking arthropods and updated Archimedes' principle. *Langmuir*, **32**, 10522–10528. https://doi.org/10.1021/acs.langmuir.6b02922

Supporting Information

Additional Supporting Information may be found in the online version of this article:

Figure S1. The dorsal side of thorax loaded by the steel cannonball sinker (arrowhead).

Figure S2. Total shadows before and after raising the forelegs, "NS" indicates not significant difference ($P > 0.05$) (*t*-test).

Figure S3. (a–d) Water striders at the rest position.

Video S1. Video clip of a water strider during raising the forelegs.

Video S2. Video clip of a water strider sculling, side view.

Video S3. Video clip of a water strider sculling, below view.

Appendix S1.